Philosophical Magazine, 1 Nov–1 Dec 2003
Vol. 83, Nos. 31–34, 3705–3721

Taylor & Francis
Taylor & Francis Group

Parametric dislocation dynamics of anisotropic crystals

X. Han, N. M. Ghoniem† and Z. Wang

Department of Mechanical and Aerospace Engineering, University of California, Los Angeles, California 90095-1597, USA

[*Received 22 July 2002 and accepted 18 May 2003*]

Abstract

Efficient computational methods for the elastic field, self force and interaction forces of three-dimensional (3D) dislocations in anisotropic elastic crystals are developed for 3D dislocation dynamics (DD). The elastic field of a general dislocation loop is determined by incorporating numerically evaluated derivatives of Green's functions in the fast sum method of Ghoniem and Sun. Self-forces of dislocation loops are calculated by numerical integrations performed on the dislocation line, and several approximation methods to the full integration are also explored. Strong effects of elastic anisotropy on many ingredients of DD are shown (e.g. the elastic field, self-forces, operation of Frank–Read sources, dipole formation and break-up and dislocation junction strength). Large-scale 3D DD simulations are carried out for copper single crystals. It is found that the dislocation microstructure and strain-hardening behaviour are also strong functions of elastic anisotropy.

§1. Introduction

The lack of physical reality in the continuum theory of plasticity makes it difficult to extrapolate with confidence the experimental database outside its range of measurements. It also fails to capture the fundamental nature of heterogeneous plasticity on the microscale and does not provide a successful framework for determination of inherent length scales that are often experimentally observed. Moreover, critical phenomena associated with flow localization in plastically deforming metals under high-strain-rate or high-stress conditions are not well predicted. Two approaches have recently emerged to address this state of affairs:

(i) the dislocation DD approach (for example Amodeo and Ghoniem (1990a, b), Kubin *et al.* (1992), Rhee *et al.* (1998), Verdier *et al.* (1998), Ghoniem and Sun (1999) and Schwarz (1999)) for direct numerical simulations of the dynamics of dislocation ensembles;
(ii) the statistical mechanics approach (for example, Glazov and Laird (1995), Gregor *et al.* (1997), Zaiser *et al.* (1998) and Trochidis *et al.* (2000)), where the evolution of dislocation populations is described by reactions (e.g. generation and annihilation) and diffusion–drift rate equations.

† Email: ghoniem@ucla.edu.

Philosophical Magazine ISSN 1478–6435 print/ISSN 1478–6443 online
http://www.tandf.co.uk/journals
DOI: 10.1080/14786430310001599531

In the DD approach, the elastic field of dislocation ensembles is determined within the simulation volume, and the local Peach–Kohler force and self-force on dislocation segments are computed. The integrated resultant force is used to determine the velocity of the dislocation segment. Several solution methods for the evolution of the dislocation microstructure have already been developed (for example Kubin *et al*. (1992), Rhee *et al*. (1998) and Schwarz (1999)). Utilizing parametrized space curves to describe the topology of dislocation lines, Ghoniem and co-workers (for example Ghoniem and Sun (1999), Ghoniem *et al*. (2000) and Huang and Ghoniem (2002)) have developed the method of parametric dislocation dynamics (PDD). The method is highly accurate and computationally efficient.

As a result of the considerable increase in computational complexity, the majority of approaches are based on isotropic elasticity. Recently Rhee *et al*. (2001) provided an approach to incorporate anisotropic elasticity into DD simulations, and Shenoy *et al*. (2000) employed anisotropic elasticity in the study of dislocation junctions in fcc metals. It is noted that earlier efforts on the determination of the equilibrium shape of dislocation loops in anisotropic crystals date back to the work of Scattergood and Bacon (1974, 1975, 1982). Since some materials possess a large degree of elastic anisotropy (e.g. ionic crystals, some metals (e.g. copper) and some covalent materials (e.g. GaAs)), it is of interest to extend the DD method to model the deformation of elastically anisotropic materials, particularly for thin-film and single-crystal applications.

For a finite straight dislocation, the elastic field can be explicitly obtained through the evaluation of a sextic equation or line integration (Willis 1970, Barnett 1972, Asaro *et al*. 1973, Mura and Mori 1976). Utilizing the results for a straight segment, Willis (1970) derived a line integral expression for a curved dislocation loop. Mura (1963) also developed a line integral for the stress field of an arbitrarily curved dislocation loop. Other procedures for the elastic field of anisotropic crystals were also developed by a number of investigators. Indenbom and Orlov (1968) obtained a solution for a curved dislocation loop, which contains higher derivatives of the straight dislocation solution. On the other hand, Lothe (1967) and Brown (1967) developed alternate solutions for the in-plane field of a planar loop. The general anisotropic theory of dislocations has been discussed by Bacon *et al*. (1980), Hirth and Lothe (1982) and Mura (1987).

One other main ingredient in DD simulations is the evaluation of the dislocation self-force, which results from the interaction force on a dislocation segment caused by all other parts of the dislocation loop. Evaluation of the self-force can be numerically taxing, since the stress field at points on the dislocation line is singular (according to classical linear elasticity). To avoid this singularity, several approximate methods have been proposed. In the finite-core approximation, a region around the point where the self-force is determined is removed from the line integrals. The Brown (1964) averaging procedure, on the other hand, is used to regularize the stress singularity. Because of the numerical overhead in calculating self-forces, a simple line tension approximation is often used.

The objectives of this work are:

(i) to extend the PDD framework to crystals of general elastic anisotropy (APDD);
(ii) to examine the influence of crystal anisotropy on the physics of elementary dislocation interaction mechanisms, and

(iii) to demonstrate an application of APDD to the simulation of dislocation microstructure evolution and the stress–strain response in copper.

To this end, we develop a numerical procedure for the efficient calculation of the elastic field associated with complex dislocation loop ensembles by extending our fast sum method (Ghoniem and Sun 1999) to anisotropic crystals. Accuracy of field calculations is ascertained by comparing the results with known solutions of other methods. We also examine several approximations utilized in determining the dislocation self-force, since its evaluation represents one of the most intensive parts of APDD. The computational costs associated with such an extension will be assessed in view of the physical insight gained through comparison of key mechanisms in both isotropic and anisotropic crystals. In § 2, we present the equations for the elastic field, self-force and dislocation motion. We then examine the effects of elastic anisotropy on the elastic field and overall dislocation dynamics in § 3. Since the precise simulation of DD in anisotropic crystals will be shown to require heavy computational costs, we also present several possible approximations that can facilitate computer simulations. Finally, a comparison of a simulation of the initial stages of plastic deformation and determination of the stress–strain curve for copper using both isotropic PDD and APDD will be presented. Discussions and conclusions are given in § 4.

§ 2. Computational method

2.1. *The elastic field*

For an anisotropic linearly elastic crystal, Mura (1963) derived a line integral expression for the elastic distortion of a dislocation loop, as

$$u_{i,j}(\mathbf{x}) = \epsilon_{jnk} C_{pqmn} b_m \int_L G_{ip,q}(\mathbf{x}-\mathbf{x}') \nu_k \, \mathrm{d}l(\mathbf{x}'), \tag{1}$$

where ν_k is the unit tangent vector of the dislocation loop line L, $\mathrm{d}l$ is the dislocation line element, ϵ_{jnh} is the permutation tensor, C_{ijkl} is the fourth-order elastic constants tensor, $G_{ij,l}(\mathbf{x}-\mathbf{x}') = \partial G_{ij}(\mathbf{x}-\mathbf{x}')/\partial x_l$ and $G_{ij}(\mathbf{x}-\mathbf{x}')$ are the Green's tensor functions, which correspond to displacement component along the x_i direction at point $\mathbf{x}$ due to a unit point force in the x_j direction applied at point $\mathbf{x}'$ in an infinite medium.

It can be seen that the elastic distortion formula (1) involves derivatives of the Green's functions, which need special consideration. For general anisotropic solids, analytical expressions for $G_{ij,k}$ are not available. However, these functions can be expressed in an integral form (for example Barnett (1972), Willis (1975), Bacon *et al.* (1980) and Mura (1987)), as

$$G_{ij,k}(\mathbf{x}-\mathbf{x}') = \frac{1}{8\pi^2|\mathbf{r}|^2} \oint_{C_k} \big[-\bar{r}_k N_{ij}(\bar{\mathbf{k}}) D^{-1}(\bar{\mathbf{k}}) + \bar{k}_k C_{lpmq} (\bar{r}_p \bar{k}_q + \bar{k}_p \bar{r}_q) N_{il}(\bar{\mathbf{k}}) N_{jm}(\bar{\mathbf{k}}) D^{-2}(\bar{\mathbf{k}}) \big] \, \mathrm{d}\phi, \tag{2}$$

where $\mathbf{r} = \mathbf{x} - \mathbf{x}'$, $\bar{\mathbf{r}} = \mathbf{r}/|\mathbf{r}|$, $\bar{\mathbf{k}}$ is the unit vector on the plane normal to $\mathbf{r}$, the integral is taken around the unit circle C_k on the plane normal to $\mathbf{r}$, $N_{ij}(\mathbf{k})$ and $D(\mathbf{k})$ are the adjoint matrix and the determinant of the second-order tensor $C_{ikjl} k_k k_l$, respectively.

2.2 *Parametric description of dislocations*

We extend here the PDD method to the simulation of DD in anisotropic crystals. A dislocation loop of arbitrary three-dimensional shape is discretized into N_s curved parametric segments. For each segment j, we choose a set of generalized coordinates $q_{ik}^{(j)}$ and corresponding shape functions $\mathcal{N}_i(\omega)$ to represent the configuration of the segment, that is

$$x_k'^{(j)}(\omega) = \sum_i \mathcal{N}_i(\omega) q_{ik}^{(j)}, \tag{3}$$

where $x_k'^{(j)}(\omega)$ is the Cartesian position of a point on segment j, and ω is a suitable parameter which we restrict in the interval $0 \leqslant \omega \leqslant 1$. Specifying the parametric segments to be flexible cubic splines, the shape functions $\mathcal{N}_i(\omega)$ take the forms

$$\mathcal{N}_1 = 2\omega^3 - 3\omega^2 + 1,\ \mathcal{N}_2 = -2\omega^3 + 3\omega^2,\ \mathcal{N}_3 = \omega^3 - 2\omega^2 + \omega,\ \mathcal{N}_4 = \omega^3 - \omega^2. \tag{4}$$

Other parametric forms and details are given in the reference (Ghoniem and Sun 1999). In the present parametric case, the generalized coordinates $q_{ik}^{(j)}$ are the position and tangent vectors associated with the beginning and end nodes on segment j.

With the line element of segment j expressed in the parametric form

$$v_k \, \mathrm{d}l(\mathbf{x}') = \mathrm{d}l_k^{(j)} = x'_{k,\omega}(j) \, \mathrm{d}\omega = \mathcal{N}_{i,\omega}(\omega) q_{ik}^{(j)} \, \mathrm{d}\omega, \tag{5}$$

the elastic distortion tensor (equation (1)) can be reduced to

$$u_{i,j}(\mathbf{x}) = \epsilon_{jnk} C_{pqmn} b_m \sum_{\beta=1}^{N_s} \int_0^1 G_{ip,q}\left(\mathbf{x} - \mathbf{x}'^{(j)}(\omega)\right) x'^{(j)}_{k,\omega} \, \mathrm{d}\omega, \tag{6}$$

where N_s is the number of parametric segments. The integration for each parametric segment β can be evaluated by Gauss numerical quadrature methods.

2.3. *Forces and motion*

At a point P on a dislocation line L, the external force per unit length is obtained by the Peach–Koehler formula $\mathbf{F}^A = (\mathbf{b} \cdot \boldsymbol{\sigma}^A) \times \mathbf{t}$, where $\boldsymbol{\sigma}^A$ is the sum of the stress from an applied load and that arising from internal sources at P, $\mathbf{b}$ is the Burgers vector of the dislocation, and $\mathbf{t}$ is the unit tangent vector of the element $\mathrm{d}\mathbf{l}$. For the special and yet important case of a planar dislocation loop lying on a glide plane with unit normal $\mathbf{n}$, the glide force acts along the in-plane normal to L at P: $\mathbf{m} = \mathbf{n} \times \mathbf{t}$. The glide component F_g^A of the external force can be obtained by resolving $\mathbf{F}^A$ along $\mathbf{m}$ as

$$F_g^A = \mathbf{F}^A \cdot \mathbf{m} = \mathbf{b} \cdot \sigma^A \cdot \mathbf{n} \tag{7}$$

The in-plane self-force at the point P on the loop is also obtained in a manner similar to the external Peach–Kohler force, with an additional contribution from *stretching* the dislocation line upon a virtual infinitesimal motion (Barnett 1976):

$$F^S = \kappa E(\mathbf{t}) - \mathbf{b} \cdot \tilde{\boldsymbol{\sigma}}^S \cdot \mathbf{n}, \tag{8}$$

where $E(\mathbf{t})$ is the pre-logarithmic energy factor for an infinite straight dislocation parallel to $\mathbf{t}$: $E(\mathbf{t}) = \frac{1}{2}\mathbf{b} \cdot \Sigma(\mathbf{t}) \cdot \mathbf{n}$, with $\boldsymbol{\Sigma}(\mathbf{t})$ being the stress tensor of an infinite straight dislocation along the loop's tangent at P. $\boldsymbol{\sigma}^S$ is self-stress tensor due to the dislocation L, and $\tilde{\sigma} = \frac{1}{2}[\boldsymbol{\sigma}^S(\mathbf{P} + \epsilon\mathbf{m}) + \boldsymbol{\sigma}^S(\mathbf{P} - \epsilon\mathbf{m})]$ is the *average* self-stress at P, κ is the in-plane curvature at P, and $\epsilon = |\mathbf{b}|/2$.

Barnett (1976) and Gavazza and Barnett (1976) analysed the structure of the self-force as a sum:

$$F^{\mathrm{S}} = \kappa E(\mathbf{t}) - \kappa\left[E(\mathbf{t}) + E''(\mathbf{t})\ln\left(\frac{8}{\epsilon\kappa}\right)\right] - J(L, \mathbf{P}) + F_{\mathrm{core}}, \tag{9}$$

where the second and third terms are line tension contributions, which usually account for the main part of the self-force, while $J(L, \mathrm{P})$ is a non-local contribution from other parts of the loop, and F_{core} is due to the contribution to the self-energy from the dislocation core.

Dislocations will move under forces and are balanced by viscous dissipation. The variational form of the governing equation of motion of a dislocation loop Γ is given by (Ghoniem and Sun 1999)

$$\int_{\Gamma} (F_k^t - B_{\alpha k} V_\alpha)\, \delta r_k \, |\mathrm{d}\mathbf{s}| = 0 \tag{10}$$

where F_k^t is the sum of the Peach–Koehler force (induced by the external and internal stress fields) and the self-force, $B_{\alpha k}$ is the resistance (inverse mobility) matrix and V_α is the velocity. Details of the method can be found elsewhere (Ghoniem and Sun 1999, Ghoniem *et al*. 2000, Huang and Ghoniem 2002).

§ 3. The influence of elastic anisotropy

Before presenting numerical examples for the effects of elastic anisotropy, we should remark that the numerical accuracy of the present method has been verified by comparing with known solutions. First, we examined the accuracy of the derivatives of Green's functions and found that the results of our method agree very well with those given by Tonon *et al*. (2001). Then, to check the accuracy of the elastic field with the parametric dislocation method, we investigated the case of a circular dislocation loop, where analytical solutions are available for the stress field (Kroupa 1960) and self-forces (Gavazza and Barnett 1976) in isotropic materials. The numerical accuracy and convergence of the parametric method are found to be excellent (Ghoniem and Walgraef 2004, Walgraef and Ghoniem 2004).

In the following, the effects of elastic anisotropy on the behaviour of dislocations will be examined through a systematic study of the outcome of elementary interaction mechanisms. First the elastic field of circular dislocation loops will be determined, and the effects of anisotropy examined. We shall then discuss the effects of elastic anisotropy on elementary dislocation mechanisms. Since simulations with full elastic anisotropy are computationally demanding, we shall seek to develop isotropic approximations based on *effective* isotropic elastic moduli. To measure the degree of deviation from elastic isotropy, we use the *anisotropy ratio* A, defined in the usual manner: $A = 2C_{44}/(C_{11} - C_{12})$ (Hirth and Lothe 1982). For an isotropic crystal, $A = 1$.

3.1. *Static dislocations*

Consider a circular loop on the (111)-glide plane of a fcc crystal, with radius R and slip direction along $[\bar{1}10]$. The x and z axes are along the $[\bar{1}10]$ and [111] directions, respectively. In the figures presented here, stresses are normalized (divided) by $\mu b/R$, with $\mu = (C_{11} - C_{12})/2$ (which is the shear modulus for an isotropic material). The ratio $C_{11} : C_{12} : \mu = 5 : 3 : 1$ is used throughout.

Figure 1 shows the shear stress distribution along the slip direction on the loop plane for different anisotropy ratios. While the absolute value of the stress increases with increasing A, the effects of elastic anisotropy are seen to be more salient inside the loop, compared with the outside region. For $A \neq 1$, the crystal is not symmetric with respect to the slip direction any more, and there is a shear stress component σ_{xy} along the slip direction on the slip plane (see figure 2 (*b*)). The change in the stress magnitude and symmetry can be seen more clearly from the stress isosurfaces of figure 2, evaluated at a normalized stress component $\sigma_{zx} = 0.08$ in all cases.

To show the effects of anisotropy on dislocation interactions, we first consider the Peach–Koehler force (interaction force) on a unit dislocation element of a straight dislocation on the same slip plane and along the y direction, induced by the glide circular dislocation loop. The Burgers vectors of the circular and straight dislocations are both along the slip direction, and their values are b and b_2 respectively. Similar to the tendency of stress components, the glide component of the Peach–Koehler force is shown to increase with increasing A, as can be seen in figure 3 (*a*). It is interesting to note from figure 3 (*b*) that, while a climb force is absent

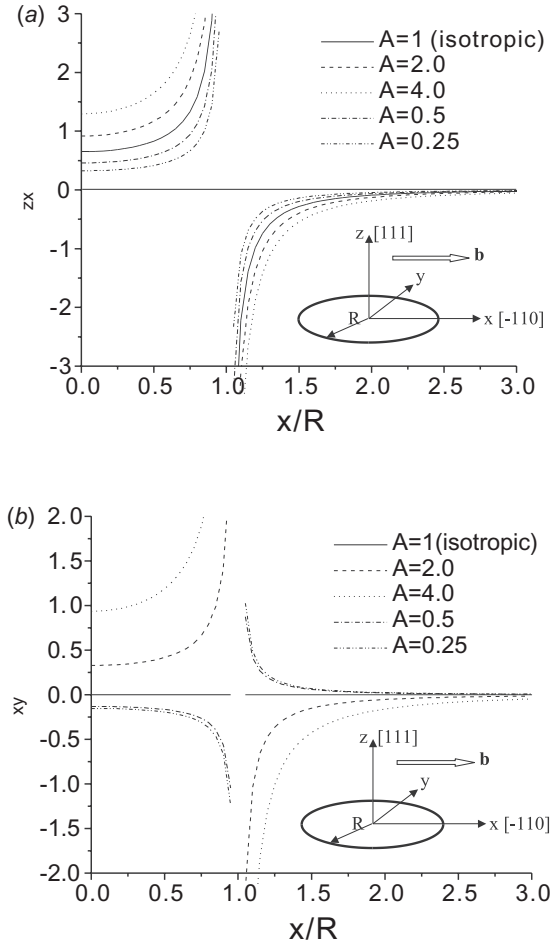

Figure 1. Stresses (normalized) along the x axis: (*a*) σ_{zx}; (*b*) σ_{xy}.

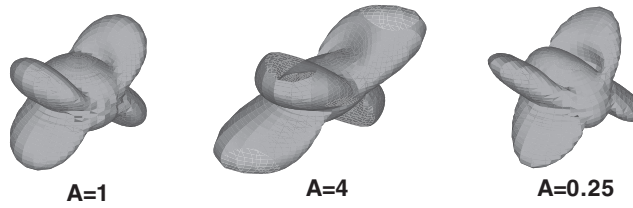

Figure 2. Isosurface of stress σ_{zx} (=0.08) for different anisotropic ratios A.

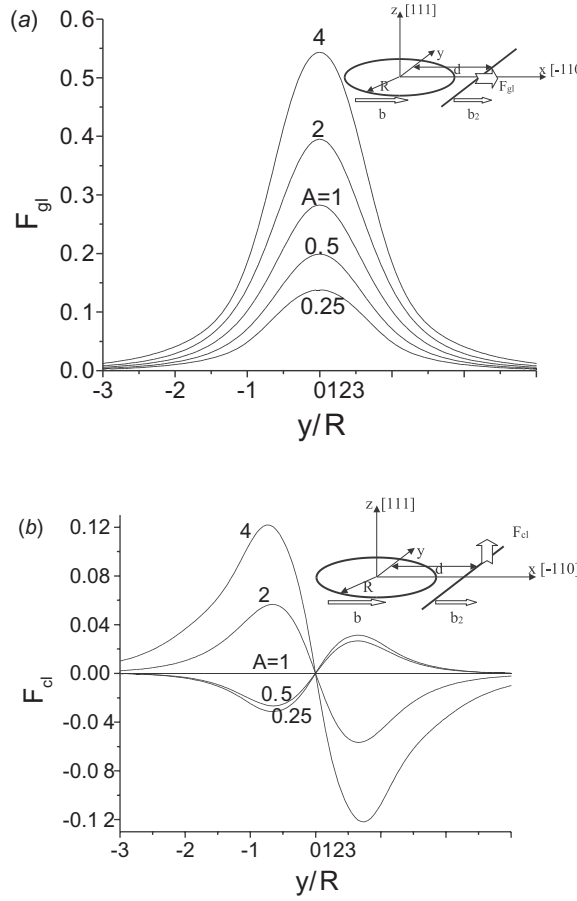

Figure 3. Peach–Koehler force (divided by $0.5(C_{11} - C_{12})bb_2/R$) of the unit dislocation element on the $z = 0$ plane and along y, with $d = 1.5R$: (*a*) glide component; (*b*) climb component.

in an isotropic crystal (i.e. $A = 1$), we find that the lack of stress component symmetry about the glide plane introduces a climb force in anisotropic crystals.

Figure 4 shows the self-force along a circular glide loop, with the loop radius $R = 100b$. The self-force is seen to increase with increasing A. For strong elastic anisotropy (e.g. in a copper crystal), the variation in the self-force along the loop is found to be considerable and non-monotonic. These examples clearly show that

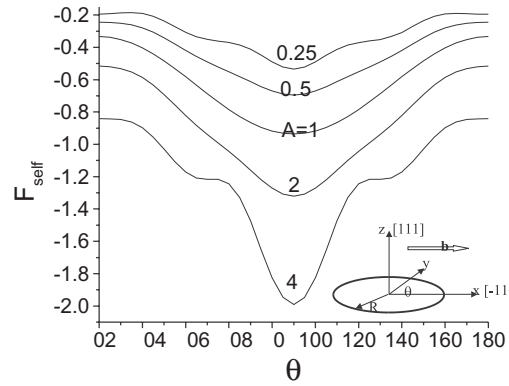

Figure 4. Self-force (divided by $0.5(C_{11} - C_{12})b/R$) along a slip circular loop, with $R = 100b$.

strong elastic anisotropy will change not only the magnitude and symmetry of the stress field but also the interaction force and self-force, sometimes in a dramatic way.

3.2. *Dislocation dynamics*

In this section, we incorporate the present methodology of calculating dislocation interactions and self-forces with full anisotropic elasticity theory into our PDD computational method (Ghoniem and Sun 1999, Ghoniem *et al.* 2000, Huang and Ghoniem 2002). We shall focus first on the results of elementary dislocation mechanisms in anisotropic cubic crystals, where the effects of anisotropy are conveniently evaluated in terms of A. The results for three typical dislocation mechanisms, essential in DD simulations, are evaluated next. These are Frank–Read (F–R) source expansion, dislocation dipoles and dislocation junctions.

Figure 5 displays the evolution of a F–R source from an initial straight segment in a fcc crystal with different anisotropic ratios A. The segment of an initial length $1000a$ is located on the (111) glide plane and is pinned at its two ends. The Burgers vector is $\mathbf{b} = \frac{1}{2}[\bar{1}01]$, and the segment is along the $[\bar{1}10]$ direction. The segment is then subjected to a sudden uniaxial stress $\sigma_{11}/\mu = 0.2\%$ (with $\mu = (C_{11} - C_{12})/2$, and resolved shear stress $\tau/\mu = 0.08\%$) along the [100] direction. Stresses are measured in units of $\mu = (C_{11} - C_{12})/2$, and distances in units of the lattice constant a. Other parameters are $C_{11} : C_{12} : \mu = 5 : 3 : 1$, and the dislocation mobility is taken as $M = 10^4\,\mathrm{Pa}^{-1}\,\mathrm{s}^{-1}$. These units and parameters will be used throughout all following simulations, unless stated otherwise.

The effects of elastic anisotropy on the expansion of a typical F–R source are shown in figure 5. As the anisotropy ratio increases, greater resistance to shear deformation is observed, as if the 'effective' self-force becomes larger. Full calculation of the self-force is computationally intensive, because of the need to perform numerical line integrals over the entire loop. Hence, local approximations become desirable. Figure 5 shows that the F–R source expansion is sensitive to the method of self-force approximation and that full calculations are required if one needs higher accuracy. This is especially evident when the F–R source expansion is unstable (see figure 5 (*b*)), because the instability threshold stress is sensitive to the magnitude of the self-force.

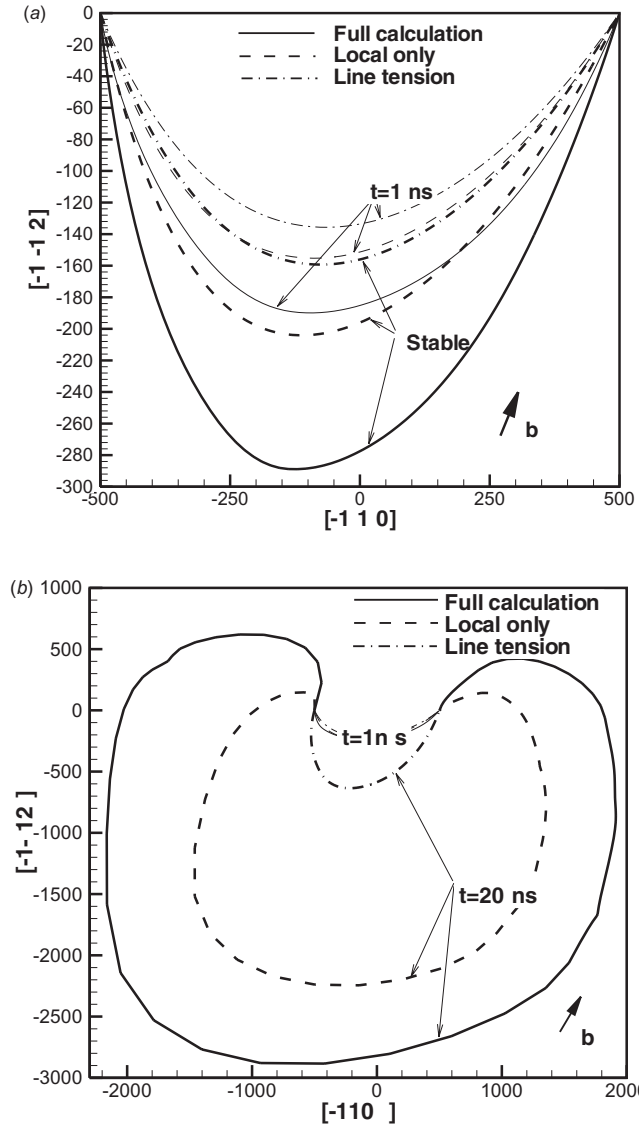

Figure 5. Evolution of a F–R source under applied stress $\sigma_{11}/\mu = 0.2\%$ (resolved shear stress $\tau/\mu = 0.08\%$, with $\mu = 0.5(C_{11} - C_{12})$), for the anisotropy ratios (*a*) $A = 2$ and (*b*) $A = 0.5$.

Next, we consider the dynamic process of dislocation dipole formation in fcc crystals. Figure 6 (*a*) shows the configurations (two-dimensionally projected on the (111) plane) of two pinned dislocation segments, lying on parallel (111) planes. The two dislocation segments, which initially are straight, parallel, and along $[\bar{1}10]$ but of opposite line directions, have the same Burgers vector $\mathbf{b} = \frac{1}{2}[\bar{1}01]$ and are pinned at both ends. Their glide planes are separated by h. In this figure, $h = 25 \times 3^{1/2}a$, $L : d : h = 800 : 300 : 25 \times 3^{1/2}$, with L and d being the length of the initial dislocation segments and the horizontal distance between them respectively. Without the application of any external loading, the two lines attract one another

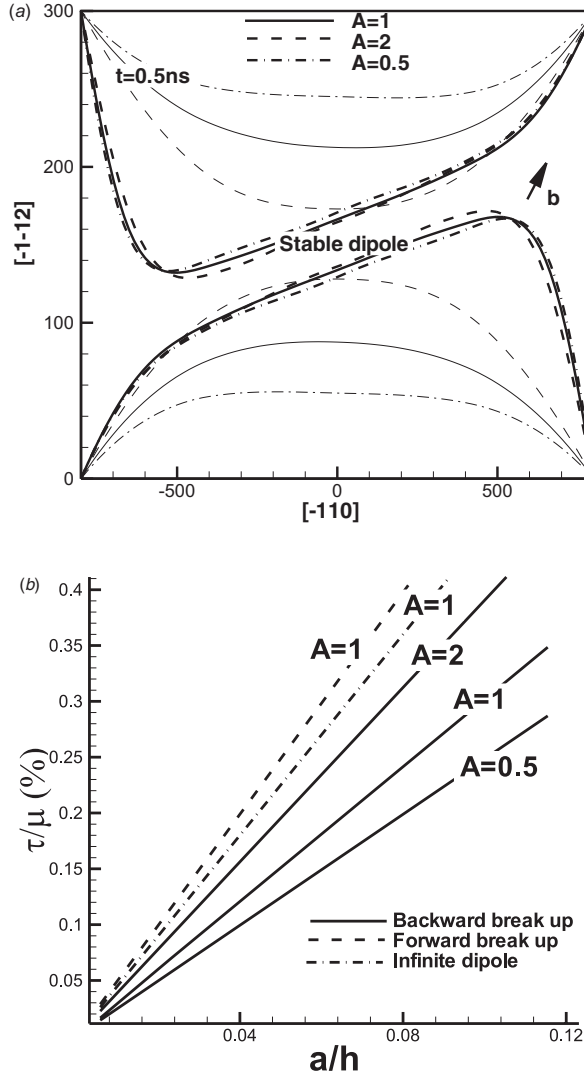

Figure 6. (*a*) Evolution of dislocation dipoles without applied loading; (*b*) break-up loadings of dipoles.

and form an equilibrium state of a finite-size dipole. It is interesting to note that, while the dynamic shape of the segments during the dipole formation is dependent on the anisotropy ratio A, the final configuration appears to be insensitive to A. Under external loading, the dipole may be unzipped, if applied forces overcome binding forces between dipole arms. The forces (resolved shear stresses τ, divided by $\mu = (C_{11} - C_{12})/2$) to break up the dipoles are shown in figure 6 (*b*). It can be seen that the break-up stress is inversely proportional to the separation distance h, consistent with the results of infinite-size dipoles. It is easier to break up dipoles in crystals with smaller A ratios (e.g. some bcc crystals). It is also noted that two ways to break up dipoles are possible: in the backward direction (where the self-force assists the break-up), or the forward direction (where the self-force opposes the

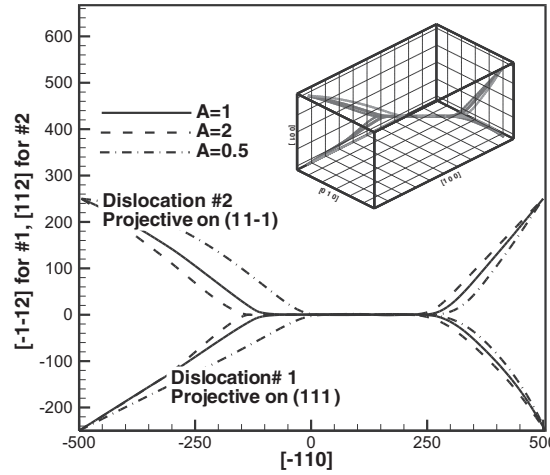

Figure 7. Evolution of dislocation junctions under applied loading $\sigma_{11}/\mu = 0.24\%$ ($\tau/\mu = 0.056\%$).

break-up). For a finite-length dipole, the backward break-up is obviously easier than the forward break-up owing to the effects of self-forces induced by the two curved dipole arms, as can be seen in figure 6 (*b*).

When two dislocations approach each other, their interaction can be very strong, leading to significant reconfiguration. They may attract each other to form a stable common part (junction), or repel one another. In figure 7, we show the configurations of attractive junctions in fcc crystals of different anisotropy ratios. Two initially straight dislocation segments, with Burgers vectors and slip planes given by $\frac{1}{2}[01\bar{1}]$ (111) and $\frac{1}{2}[101](11\bar{1})$, respectively are pinned at their ends. They are allowed to move and approach each other, until they lock in an equilibrium state. The two dislocations attract each other to form a common junction along the intersection direction of the two glide planes $[\bar{1}10]$. Each of the initial dislocations has a length of $500 \times 5^{1/2}$ and makes an angle $\theta = 26.6^\circ$ with $[\bar{1}10]$. Without the external loading, the junction configuration in crystals with different anisotropy ratios A are quite similar. The strong binding forces appear to overcome differences in their self-forces, and thus the configuration is not sensitive to A. With an increase in external loading, the junction length decreases, until the junction is unzipped at a critical stress. The junction strength is found to depend on the anisotropy ratio. From the figure, it can be seen that, under external loading, the junction length decreases more rapidly for smaller A. Dislocation junctions of the type studied here are thus weaker (or stronger) in anisotropic crystals of lower (or higher) values of A.

3.3. *Approximations with effective moduli*

Although the PDD has been extended in this work to crystals of arbitrary elastic anisotropy, in practice, however, the computational requirements can be taxing, especially in large-scale computer simulations. For that purpose, it may be advantageous to perform computer simulations with isotropic PDD, provided that the results of such simulations would closely match the more computationally intensive APDD. In this section, we investigate three different averaging methods that have been proposed to extract 'equivalent' isotropic elastic constants from the full

Table 1. Elastic constants of single-crystal copper ($C_{11} = 168.4\,\text{GPa}$, $C_{12} = 121.4\,\text{GPa}$ and $C_{44} = 75.4\,\text{GPa}$)

	μ (GPa)	ν
Voigt	54.6	0.324
Reuss	40.0	0.369
Scattergood and Bacon	42.1	0.431

anisotropic values. Two such methods, namely the Voigt and Reuss averaging procedures are common in general elastic deformation problems, while the third, the Scattergood–Bacon (1974) procedure, has been specially used in the context of determining equilibrium shear loop configurations. We shall examine here the extent of agreement between isotropic PDD with the APDD, when these three approximations are used.

In the Voigt scheme, the averaging is performed over the elastic constant tensor C_{ijkl} while, in the Reuss scheme, it is done over elastic compliances S_{ijkl}. Results of such averaging and relevant parameters for some anisotropic crystals have been listed by Hirth and Lothe (1982). All calculations reported in this section are for the case of single-crystal copper ($A = 3.21$). The calculated elastic constants are given in table 1.

First, we give a simple example, to determine how well the static stress field of dislocations in anisotropic crystals can be approximated by effective isotropic elasticity. Calculations of the stress field along the symmetry axes of a circular shear dislocation loop show that the shear stress component σ_{zx} can be well approximated (especially by the Scattergood–Bacon scheme) along the coordinate axes. However, as a result of anisotropy, a distortion stress component σ_{xy} exists even along the geometric symmetric axes, which cannot be produced by any isotropic approximation. Thus, the full components of the stress field tensor induced by dislocations in anisotropic crystals cannot be replaced by isotropic approximations. However, the influence of such difference on interaction and self-forces and on microstructure evolution needs to be investigated.

To study the effects of averaging the anisotropic elastic moduli in PDD simulations, we shall compare here the results of full anisotropic calculations with their corresponding isotropic approximations. This will be accomplished by focusing on three typical dislocation mechanisms: F–R source expansion, dipole dynamics and junction formation.

Figure 8 shows the results of DD simulations of a F–R source on the $\frac{1}{2}[\bar{1}01]\,(111)$ slip system. For stable F–R configurations below a critical bow-out stress, or at short evolution times, the isotropic approximations of Reuss and of Scattergood and Bacon are quite suitable. For stress levels greater than the critical bow-out stress, and at long time intervals, great differences exist between the approximation and the full anisotropic calculations. For the special case of the F–R source, it is found that the Scattergood–Bacon approximation is the most suitable, followed by the Reuss averaging schemes. Figure 9 shows the simulation results for the process of dipole formation. The geometries of the two initial dislocation segments and slip systems are the same as described in § 3.2. The results indicate that none of the isotropic approximations produces similar dipole configurations to the anisotropic case.

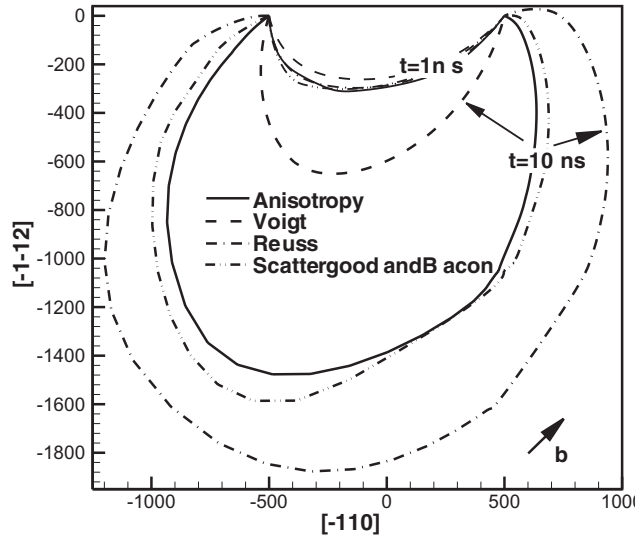

Figure 8. Evolution of a F–R source in anisotropic elasticity, compared with isotropic approximations, with applied stress $\sigma_{11} = 120\,\text{MPa}$.

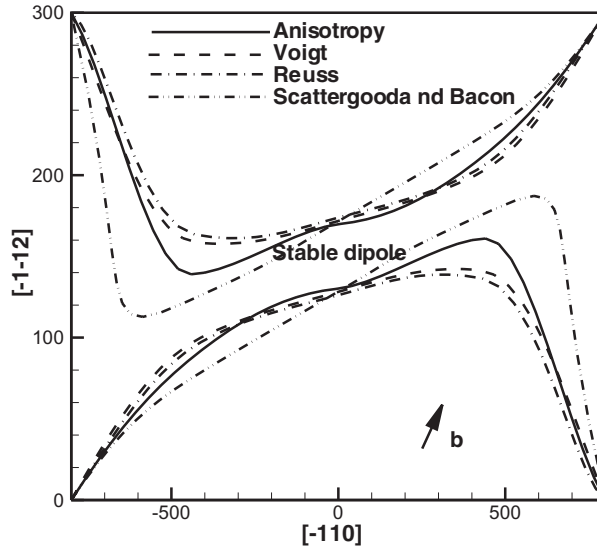

Figure 9. Dislocation dipole in anisotropic elasticity, compared with isotropic approximations, with applied loading $\sigma_{11} = 45\,\text{MPa}$.

While the middle section of the finite-size dipole is perfectly straight in the isotropic case, the lateral separation between the dipole arms is not constant in the anisotropic case. This is a consequence of the stronger dependence of the self-force on the angle between the Burgers and tangent vectors in the anisotropic case.

Finally, we show the results of computer simulations of a dislocation junction in figure 10. The junction has the same initial geometry and slip systems as given in figure 7. Without external loading, all three isotropic approximations reproduce the

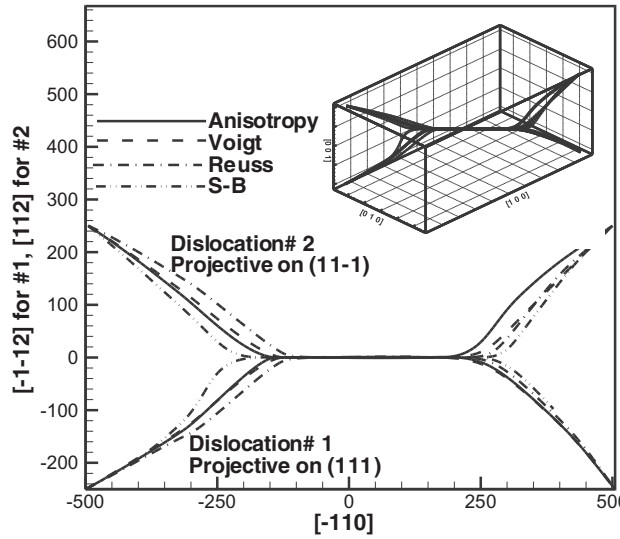

Figure 10. Dislocation junction in anisotropic elasticity, compared with isotropic approximations, with applied loading $\sigma_{11} = 80\,\text{MPa}$: S–B, Scattergood and Bacon.

anisotropic results quite well. Differences between the results of full anisotropic calculations and those of isotropic approximations increase with increasing external loading and hence give different junction strengths.

Generally, all these typical dislocation mechanisms can be captured and simulated qualitatively by isotropic approximations. The errors are on the order of about 20% or less, and the Scattergood–Bacon or Reuss approximations to the elastic moduli are preferable. However, for more accurate studies of dislocation mechanisms (e.g. in thin films), or for studies of critical stress levels to bow out a segment or to unzip dipoles or junctions, care must be exercised in using isotropic approximations.

3.4. *Strain hardening in copper*

In contrast with our PDD computer code using isotropic elastic theory, APDD simulations are computationally massive. The main reason is that the evaluation of the elastic field and self-forces requires additional numerical integrations, with a corresponding large number of calculations of the derivatives of Green's functions. To reduce the computational cost, a storage and look-up table technique can be used. We calculate the functions $G_{ij,k}(\mathbf{r})/r^2$, which only depend on the unit direction vector $\mathbf{r}/r$ at tabulated data points (usually represented in spherical coordinates). We then store the results of these calculations in a look-up table. Values of these functions at desired directions are obtained by interpolation. This technique results in higher demands on memory allocations but is generally advantageous for massive DD simulation. When computing and storing these functions, we also take advantage of the symmetry properties: $G_{ij,k}(\mathbf{r}) = G_{ji,k}(\mathbf{r}) = -G_{ij,k}(-\mathbf{r})$. This symmetry reduces the number of Green's derivative components from 27 to 18. The functions $G_{ij,k}(\mathbf{r})/r^2$ were first evaluated at points on a half-unit sphere, represented by the two angles $0 \leqslant \theta \leqslant \pi/2$ and $0 \leqslant \phi \leqslant 2\pi$. Values at intervals $\Delta\theta = \Delta\phi = h$ have been calculated and stored, and a linear interpolation scheme was then used to determine

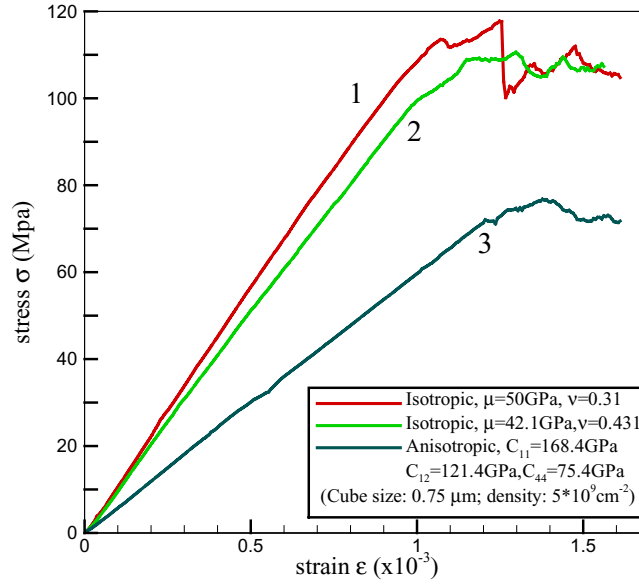

Figure 11. Stress–strain curve simulation for a copper single crystal.

other function values. We chose $h = \pi/500$, resulting in storage requirements for 4.5×10^6 function evaluations.

To study the effects of elastic anisotropy on strain hardening and the corresponding dislocation microstructure evolution, the deformation of a copper cube of side 0.75 μm and containing an initial dislocation density of $5 \times 10^{13}\,\mathrm{m}^{-2}$ is simulated. An initial random distribution of 40 dislocation loops was generated on different slip planes. Periodic boundary conditions were applied to loops that expand beyond the simulation volume boundary such that segments which leave one of the surfaces are mapped back periodically on corresponding entry points on opposite surfaces. In these calculations, we simulate a uniaxial tensile test of the cube at a constant strain rate $10^3\,\mathrm{s}^{-1}$, with the load applied along [100] direction.

The corresponding simulated stress–strain curve is shown in figure 11, where calculations with full elastic anisotropy are compared with the Voight and Scattergood–Bacon approximations. It is clear that neither approximation is capable of reproducing the stress–strain curve for anisotropic single crystals. A major difference is attributed to the elastic response at very low strains as a result of differences in the 'effective Young's modulus'. If this difference is accounted for, one can see that the strain hardening behaviour that results from dislocation microstructure is reproduced somewhat better by the Scattergood–Bacon approximation. These observations are derived from simulations to low strain values, while simulations at high strains or different microstructures may reveal other features.

§4. Discussion and conclusions

The PDD for computer simulations of mesoscopic plastic deformation in isotropic elastic materials has been extended in this work to crystals of general elastic anisotropy. This has been based on incorporation of numerically evaluated Green's functions and their derivatives in fast numerical quadrature sums representing line integrals. The procedure, although computationally more intensive than the original

PDD, has been demonstrated to be accurate and numerically convergent. The substantial computational expense is a direct result of the need to perform multiple integrals (rather than single integrals) for Peach–Kohler and self-force calculations to update nodal coordinates. Numerical integrals are needed for the derivatives of Green's functions as well as line integrals over each dislocation loop. In large-scale computer simulations, a computational technique based on symmetry, storage, table look-up and interpolation for the derivatives of Green's functions has resulted in the alleviation of some of the computational burden. The following conclusions are drawn from the present study.

(1) The stress fields, dynamic process and critical conditions (such as for F–R source operation, junction unzipping and dipole unzipping) of dislocations are sensitive to the anisotropy ratio. While the equilibrium configurations of dislocations, such as dipoles or junctions, appear to be insensitive to it.
(2) Generally, the three typical dislocation mechanisms (F–R sources, dipoles and junctions) can be captured and simulated qualitatively by isotropic approximations. The errors are of the order of 20% or less, and the Scattergood–Bacon or Reuss approximations is preferable. However, for more accurate or critical state studies, care must be exercised in using isotropic approximations. There is no *a priori* obvious isotropic approximation for each type of dislocation mechanism. Case-by-case comparisons with full anisotropic calculations are essential before a particular isotropic approximation is used.
(3) The stress–strain behaviour of highly anisotropic single crystals (e.g. copper) cannot be reproduced by equivalent isotropic approximations.

Acknowledgements

This research is supported by the National Science Foundation under grant NSF-DMR-0113555 with UCLA, University of California, Los Angeles.

References

Amodeo, R. J., and Ghoniem, N. M., 1990a, *Phys. Rev.*, **41**, 6958; 1990b, *ibid.*, **41**, 6968.
Asaro, P., Hirth, J., Barnett, D., and Lothe, J., 1973, *Phys. Stat. sol.* (b), **60**, 261.
Bacon, D., Barnett, D., and Scattergood, R., 1980, *Prog. Mater. Sci.*, **23**, 51.
Barnett, D., 1972, *Phys. Stat. Sol.* (b), **49**, 741; 1976, *Phys. Stat. sol.* (a), **38**, 637.
Brown, L., 1964, *Phil. Mag.*, **10**, 441; 1967, *ibid.*, **15**, 363.
Gavazza, S., and Barnett, D., 1976, *J. Mech. Phys. Solids*, **24**, 171.
Ghoniem, N. M., and Sun, L. Z., 1999, *Phys. Rev.* B, **60**, 128.
Ghoniem, N. M., Tong, S.-H., and Sun, L. Z., 2000, *Phys. Rev.*, **61**, 913.
Ghoniem, N., and Walgraef, D., 2004, *Instabilities and Self-Organization in Materials*, II, *Applications* (Dordrecht: Kluwer).
Glazov, M., and Laird, C., 1995, *Acta metall. mater.*, **43**, 2849.
Gregor, V., Kratochvil, J., and Saxlova, M., 1997, *Mater. Sci. Engng*, **A234–A236**, 209.
Hirth, J., and Lothe, J., 1982, *Theory of Dislocations* (New York: Wiley).
Huang, J., and Ghoniem, N., 2002, *Modelling Simulation Mater. Sci. Engng*, **10**, 1.
Indenbom, V., and Orlov, S., 1968, *J. appl. Math. Mech.*, **32**, 414
Kroupa, F., 1960, *Czech. J. Phys.* B, **10**, 284.
Kubin, L. P., Canova, G., Condat, M., Devincre, B., Pontikis, V., and Brechet, Y., 1992, *Diffusion Defect Data—Solid St. Data* B, **23–24**, 455.
Lothe, J., 1967, *Phil. Mag.*, **15**, 353.

Mura, T., 1963, *Phil. Mag.*, **8**, 843; 1987, *Micromechanics of Defects in Solids* (Dordrecht: Martinus Nijhoff).
Mura, T., and Mori, T., 1976, *Phil. Mag.*, **33**, 1021.
Rhee, M., Stolken, J., Bulatov, V., Diaz de la Rubia, T., Zbib, H., and Hirth, J., 2001, *Mater. Sci. Engng*, **A309–A310**, 288.
Rhee, M., Zbib, H., Hirth, J., Huang, H., and Diaz de la Rubia, T., 1998, *Modelling Simulation Mater. Sci. Engng*, **6**, 467.
Scattergood, R., and Bacon, D., 1974, *Phys. Stat. sol.* (a), **25**, 395; 1975, *Phil. Mag.*, **31**, 179; 1982, *Acta Metall.*, **30**, 1665.
Schwarz, K., 1999, *J. appl. Phys.*, **85**, 108.
Shenoy, V., Kukta, R., and Phillips, R., 2000, *Phys. Rev. Lett.*, **84**, 1491.
Tonon, F., Pan, E., and Amadei, B., 2001, *Comput. Struct.*, **79**, 469.
Trochidis, A., Douka, E., and Polyzos, B., 2000, *J. Mech. Phys. Solids*, **48**, 1761.
Verdier, M., Five, M., and Groma, I., 1998, *Modelling Simulation Mater. Sci. Engng*, **6**, 755.
Walgraef, D., and Ghoniem, N., 2004, *Instabilities and Self-Organization in Materials*, I, *Fundamentals* (Dordrecht: Kluwer).
Willis, J., 1970, *Phil. Mag.*, **21**, 931; 1975, *J. Mech. Phys. Solids*, **23**, 129.
Zaiser, M., Avlonitis, M., and Aifantis, E., 1998, *Acta mater.*, **46**, 4143.